Distributionally Robust Service Restoration for Integrated Electricity-heating Systems Considering Secondary Strikes of Subsequent Random Events

Yumian Lin[a], Houbo Xiong[a], Yue Zhou[b], Tianjing Wang[c], Yujie Lin[a], Chuangxin Guo[a]

[a]*College of Electrical Engineering, Zhejiang University, Hangzhou 310027, China*
[b]*School of Engineering, Cardiff Universit, Cardiff CF24 3AA, UK*
[c]*School of Electrical and Electronic Engineering, Nanyang Technological University, Singapore*

Highlights

- A novel SR strategy is designed, incorporating a comprehensive optimization of multiple schemes to pick up important load.
- The virtual energy storage of the DHN is utilized as an emergency resource in the SR process.
- An ambiguity set and support set combined DRO model is presented.
- Logical constraint convex relaxation and an improved C&CG algorithm is developed.

Keywords:

Integrated electricity-heating system; Service restoration; Virtual energy storage; Ambiguity set and support set; Secondary strike; Distributionally robust optimization

Abstract

The multi-energy system has become a pivotal technology for achieving zero-carbon transition. To address the extreme events with increasing frequency, this paper proposes a novel service restoration (SR) strategy for the integrated electricity-heating system to effectively restore critical loads after such events. The novel SR strategy encompasses defensive microgrid reconfiguration, mobile emergency generators allocation, and reserve commitment. Besides, the virtual energy storage of the heating system is utilized as an emergency resource in the SR process. By modeling the uncertain failures with a combination of ambiguity sets and support sets, the proposed SR strategy can effectively manage secondary strikes from subsequent random events. A distributionally robust optimization (DRO) model is then presented to identify the worst-case probability distribution of these uncertainties, enabling robust restoration decisions. To solve the DRO model efficiently, this paper proposes a solution method that employs logical constraint relaxation to tackle the non-convex challenges posed by discrete decision variables. Additionally, an improved column and constraint generation algorithm is developed. Case studies on modified 6-bus and 6-node systems, as well as IEEE 33-bus and 32-node systems, demonstrate the effectiveness of the proposed model and solution methodology.

1. Introduction

Due to rapid environmental changes, high-impact and low-probability natural disasters, such as hurricanes, floods, wildfires, and extreme weather events, have caused significant power outages over recent decades. Statistics from 2003 to 2012 indicate that 58% of power outages in the United States were attributable to natural disasters, resulting in annual economic losses ranging from $18 billion to $33 billion [1]. *Typhoon Lekima* in 2019 significantly impacted southeastern China, causing extensive infrastructure damage and disruptions that persisted for several days [2]. Similarly, in 2020, ice storms in Jilin Province, northeastern China, led to the shutdown of major thermal power plants due to disruptions in lines and pipelines, affecting over 300 million people with shortages of electricity and heating [3]. In the United States, the severe cold wave in 2021 resulted in nearly 10 million people losing access to natural gas and electricity during peak hours, with estimated economic losses up to $295 billion [4]. These incidents underscore the vulnerabilities of the electrica

* *Corresponding author.*
E-mail address: author@institute.xxx

Nomenclature

Abbreviations

IEHS	Integrated electricity-heating system
PDS	Power distribution system
DHN	District heating network
MG	Microgrid
VES	Virtual energy storage
SR	Service restoration
CHP	Combined heat and power
EH	Electric heater
MEG	Mobile emergency generator
SP	Stochastic programming
RO	Robust optimization
DRO	Distributionally robust optimization

Indices and sets

i, $\mathcal{B}$	Index, set of buses
l, $\mathcal{L}$	Index, set of branches
m, $\mathcal{M}$	Index, set of MGs
n, $\mathcal{N}$	Index, set of nodes
s, $\mathcal{S}$	Index, set of thermal sources
e, $\mathcal{E}$	Index, set of thermal loads
p, $\mathcal{P}$	Index, set of pipelines
c, $\mathcal{C}$	Index, set of CHPs
h, $\mathcal{H}$	Index, set of EHs
g, $\mathcal{G}$	Index, set of MEGs
w, $\mathcal{W}$	Index, set of wind turbines
d, $\mathcal{D}$	Index, set of power loads

Parameters

q_K, α_K	the kth mass blocks
τ_1, τ_2, τ_p	The weighted average of temperatures of mass blocks
C^{P}	Specific heat capacity of DHN heating medium
T_t^{A}	Ambient temperature
λ_p, L_p	Loss efficient and length of pipe p
p_s, Ns	Probability of scenario s and number of scenarios
Ξ	Support set of random variables
$\hat{\mathbb{P}}$, $\hat{\boldsymbol{\xi}}$	Empirical distribution and historical fault obey the distribution
c_c^{suc}, c_c^{sdc}, c_c^{onc}	The Start-up/Shut-down/no-load cost of CHP c
T_c^{on}, T_c^{off}	Minimum on/off time of CHP c
$P_{c,\max}^{\mathrm{CHP}}$, $P_{c,\min}^{\mathrm{CHP}}$	Upper/lower power limit of CHP c
$P_{h,\max}^{\mathrm{EH}}$, $P_{h,\min}^{\mathrm{EH}}$	Upper/lower power limit of EH h
$P_{g,\max}^{\mathrm{MEG}}$, $P_{g,\min}^{\mathrm{MEG}}$	Upper/lower power limit of MEG g
C_d^{Loss}, C_n^{Loss}	Penalty cost of load shedding at bus d and node n
$A_{w,t}^{\mathrm{WT}}$	Available wind power capacity
$P_{d,t}^{\mathrm{L}}$, $Q_{d,t}^{\mathrm{L}}$, $H_{n,t}^{\mathrm{L}}$	Active power/passive power/thermal load demand at bus d and node n at stage t
$\overline{V}_i$, $\underline{V}_i$	Upper/lower bound of voltage amplitude at bus i
$\overline{Pf}_l$, $\overline{Qf}_l$	Active/passive power flow limit of branch l
x_l, r_l	Reactance and resistance of branch l
RU_c^{CHP}, RD_c^{CHP}	Ramp up/down rate limit of CHP c
RU_h^{EH}, RD_h^{EH}	Ramp up/down rate limit of EH h
RU_g^{MEG}, RD_g^{MEG}	Ramp up/down rate limit of MEG g
$m_{p,t}^{\mathrm{s/r}}$, $m_{n,t}$	Mass flow of supply/return network in pipe p and node n at stage t

Variables

$x_{i,m}$, $y_{l,m}$	Binary status of bus i and branch l in MG m
Sw_l	Binary variables of switch status in branch l
g_i	Root bus i
f_l	The fictious flow in branch l
$\mathbb{P}$, $\boldsymbol{\xi}$	Real distribution and random variables obey the distribution
Π	Joint distribution of $\boldsymbol{\xi}$ and $\hat{\boldsymbol{\xi}}$ on the support set of $\Xi\times\Xi$ whose marginal distributions is $\mathbb{P}$ and $\hat{\mathbb{P}}$.
$u_{c,t}$, $v_{c,t}$, $i_{c,t}$	The Start-up, Shut-down and online indicator variables of CHP/MEG c/g at stage t
$\overline{P}_{c,t}^{\mathrm{CHP}}$, $\underline{P}_{c,t}^{\mathrm{CHP}}$	Upper/lower active power bound of servers service on CHP c at stage t
$\overline{P}_{h,t}^{\mathrm{EH}}$, $\underline{P}_{h,t}^{\mathrm{EH}}$	Upper/lower active power bound of servers service on EH h at stage t
$\overline{P}_{g,t}^{\mathrm{MEG}}$, $\underline{P}_{g,t}^{\mathrm{MEG}}$	Upper/lower active power bound of servers service on MEG g at stage t
$P_{c,t}^{\mathrm{CHP}}$, $Q_{c,t}^{\mathrm{CHP}}$	Active power/passive power output of CHP c at stage t
$P_{h,t}^{\mathrm{EH}}$	Input of EH h at stage t
$P_{g,t}^{\mathrm{MEG}}$, $Q_{g,t}^{\mathrm{MEG}}$	Active power/passive power output of MEG g at stage t
$P_{w,t}^{\mathrm{WT}}$	Consumed wind power of WT w at stage t
$Pf_{l,t}$, $Qf_{l,t}$	Active power flow/passive power flow of branch l at stage t
$z_{l,t}$	The status of branch l at stage t
$V_{i,t}$	The voltage amplitude of bus i at stage t
$H_{c,t}^{\mathrm{CHP}}$	Thermal output of CHP c at stage t
$H_{h,t}^{\mathrm{EH}}$	Thermal output of EH h at stage t
$T_{n,t}^{\mathrm{s/r}}$, $T_{n,t}^{\mathrm{s/r,mix}}$	The (mix) temperature of node n in the supply/return network at stage t
$T_{p,t}^{\mathrm{s/r,out}}$, $T_{p,t}^{\mathrm{s/r,in}}$	The inlet/outlet temperature of pipe p in the supply/return network at stage t
$P_{d,t}^{\mathrm{Loss}}$, $Q_{d,t}^{\mathrm{Loss}}$, $H_{n,t}^{\mathrm{Loss}}$	The active power/passive power shedding of bus d and thermal load shedding of node n at stage t

grid to extreme events, highlighting the need for proactive measures to enhance grid resilience, minimize forced load shedding, and expedite SR following such disruptions.

The SR prioritizes the protection of critical loads and the repair of faulty components, which include MG reconfiguration/integration [5-10], operation of switches [11-12], dispatch of MEG [13-18], and routing of repair crews [19]. Among the above strategies, MG reconfiguration is notably significant, primarily because it prioritizes continuity of supply over immediate repair. Maintaining a radial topology within the MG is a fundamental requirement for reconfiguration [5]. The process of MG reconfiguration is not only constrained by the radial operation of the distribution systems but also requires components that control the frequency and voltage stability within the isolation area. Mobile sources, as a flexible component with voltage regulation capabilities, participate in the process of SR to extend the survival time of critical loads. Mobile sources including generators [14], storage systems [15] and electric vehicles [16] are managed and guided to ensure the continuous power supply of critical loads. Among them, the MEG can further participate in the SR strategy including black start due to its continuous and controllable supply capability [17].

While existing studies employ the coordination of MG configuration and MEG allocation to ensure the continuous supply of power distribution systems (PDS), they often ignore the impact of secondary strikes from subsequent random events. For instance, Hurricane Sandy disrupted New York State's power system on October, 2012, leaving more than 2 million customers without power at its peak and triggering a series of subsequent

incidents in the following days, including natural gas pipelines ruptures and damage to emergency power sources, ultimately leaving some areas without energy for over a week [20]. Similarly, Hurricane Harvey in 2017 struck Texas, leaving over 338,000 electricity customers without power. Full restoration took a week, as flooding from secondary disasters significantly impeded recovery efforts [21]. In the 2019 typhoon in the Tokyo area, the extended duration of the storm led to secondary strikes, causing further disruptions [23]. Secondary strikes can cause load shedding through sudden interruption of the energized branch, disrupting the original SR strategy. Therefore, to further enhance the risk resistance of the SR strategy under prolonged extreme events, the secondary strikes should be considered. Moreover, it is worth noting that reserve commitment is maturely applied in normalized dispatch [24] and pre-extreme event unit commitment [25] to solve the uncertainty problem of renewable energy and extreme event. In the research of reserve participation in SR, significant attention is given to the economic evaluation and scheduling of reserve commitment in day-ahead frequency SR market [26-27]. However, the significance of reserve commitment to SR during subsequent random event is ignored, particularly when considering the integration of MG reconfiguration and MEG allocation.

With the advent of smart grid technology, multi-energy systems are widely constructed for achieving efficient zero-carbon transition. The widespread adoption of coupled components, such as combined heat and power (CHP) units, has promoted the integration of PDS with the district heating network (DHN) into IEHS. While this integration enhances operation flexibility and brings economic benefits for power systems, it also introduces challenges to the SR process, such as limited energy conversion efficiency of CHP and load shedding propagation from PDS to DHN [3]. To address these challenges, the remote control of IEHS is used to adjust the topology of PDS and the configuration of DHN [28]. Similar studies of SR for IEHS are conducted in [29-30].

Although the above studies have investigated achieving a continuous supply of services through approaches such as reconfiguration and compensating for the lack of CHP flexibility, they have ignored the storage capacity provided by pipelines through the thermal inertia characteristics of DHN, also called virtual energy storage (VES), which offers a crucial flexibility resource for SR. Ref. [31] simulates the hysteresis phenomenon of the thermal network using the node method and describes the thermal storage characteristics of the pipeline. Ref. [32] recognized the role of pipeline storage in improving SR capacity but modeled it as centralized energy storage, ignoring the actual physical limitations of pipeline storage. The VES has also been used to reduce operating costs [33] but has not been applied in SR, indicating an area that needs improvement.

The mentioned studies have adopted deterministic optimization methods for SR, but the occurrence of natural disasters and secondary strikes are hard to predict. Stochastic programming (SP) and robust optimization (RO) are employed to enhance the system's ability to handle uncertainty, thereby improving the reliability of SR strategies [14-16,34]. While SP can effectively model various uncertainties, it necessitates accurate probability distributions. Obtaining these distributions of independent events, such as branch outages, is challenging and can lead to a significant increase in problem dimensionality, thereby reducing solution efficiency [29]. In contrast, RO does not rely on modeling probability distributions or uncertainty-related information. Instead, it conceptualizes extreme events as adversaries to develop a robust SR strategy [35]. However, the resulting strategy may have lower cost efficiency.

Distributionally robust optimization (DRO) is a novel decision-making approach that differs from RO, which only relies on the worst-scenario boundary values of uncertain variables, and from SP, which requires numerous samples to simulate potential distribution. The DRO model describes uncertainty by defining an ambiguity set that encompasses all potential distributions at a certain confidence level and combining it with a support set that specifies the possible range of values [36]. This approach allows the DRO model to overcome its reliance on precise distributions or extreme scenarios. It seeks the worst-case distribution within an ambiguity set containing a large number of possible distributions, while restricting specific events conformed to the distribution within the defined support set. However, most exiting DRO-based energy system optimization models use first-order and second-order moments to capture the high-dimensional trends of distribution [37-38]. Some studies employ divergence-based modeling, but its asymmetric nature leads to incomplete decisions [39]. Consequently, many studies focus on DRO under the Wasserstein metric, which has demonstrated advantages in various tasks , including conventional scheduling of IEHS [40], resilience improvement [41], and pre-disaster preparation [42]. Unfortunately, there is no study applying the DRO model in SR strategy formulation in the context of secondary strikes, which are likely to occur and challenging to predict. We aim to develop a DRO-based SR strategy that utilizes the advantages of DRO model in addressing uncertainty, resulting in a high computational efficiency (ability to manage greater potential uncertainties with a low computational burden) and high solution quality (effective use of historical data sets and compatibility with multiple SR strategies) in SR strategy process.

The main contributions of this paper are listed as follows and are compared with the existing studies in Table 1.

1) We propose a novel SR strategy for IEHS, that comprehensively integrates defensive MG reconfiguration, MEG allocation and reserve commitment. This strategy aims to ensure the continuous supply of critical loads during SR. By incorporating the uncertainty of secondary strikes of subsequent random events, the proposed novel strategy enhances the survivability of critical loads throughout the SR implementation process.

2) We model the thermal inertia of the DHN as VES and integrate it into the implementation process of SR strategy as an emergency resource, which can enhance the flexibility reserve before secondary strikes, thereby reducing the thermal load shedding in DHN after IEHS is impacted.

3) An ambiguity set and support set combined DRO model is utilized to capture the uncertainty of secondary strikes in the IEHS. The ambiguity set describes the potential distributions, including the worst-case distribution of secondary strikes, while the support set defines the boundaries of the outage events.

4) The DRO model is formulated by a two-stage tri-level problem, which is further decomposed into a SR implementation master problem and several subproblems screening out the worst-case uncertainty distribution. A customized convex relation technology is introduced to guarantee the tractability of proposed DRO model, and an improved column and constraint generation (C&CG) algorithm is developed to efficiently obtain optimal solutions.

Table 1
Comparative features of relevant studies pertaining to SR strategies for IEHS

Reference	Secondary strikes	VES	MG reconfiguration	MEG allocation	Reserve commitment	Uncertainty
[14]	✓	×	✓	✓	×	✓
[6,15-16]	×	×	✓	✓	×	✓
[10,18]	×	×	✓	✓	×	×
[9,11,19]	×	×	✓	×	×	×
[7,22]	✓	×	✓	✓	×	✓
[12,25]	×	×	✓	×	✓	✓
[3,17,28]	×	×	×	✓	×	✓
[30,32]	×	✓	×	×	×	×
This work	✓	✓	✓	✓	✓	✓

2. Concept of SR Strategy for IEHS

This section mainly introduces the concept of the proposed SR strategy and DRO model. Section 2.1 describes the SR framework, integrating multiple strategies and the method for capturing subsequent fault uncertainty. Then, section 2.2 introduces the VES formulation resulting from thermal inertia of the IEHS. Finally, section 2.3 explains the construction of the ambiguity set and support set for the DRO model.

2.1 Framework of Proposed SR Strategy

During extreme events, the electricity transmission system is initially impacted, causing the main grid to experience a decline in supply capacity. To ensure the stable operation of the main grid, it is necessary to reduce or cut off the power supply on the interconnection line in the fault area. This paper focuses on the IEHS in the fault area and develops a more robust and economical integrated SR strategy for such scenarios. This proposed strategy captures the uncertainty of secondary strikes of subsequent random events through the DRO model and improves the risk resistance of the SR strategy.

Fig. 1 is taken as an example to illustrate the framework for formulating and implementing SR strategies for the IESH, which consists of the PDS, DHN, CHP units, and electric heater (EH) units. After an extreme event, the substation of the IEHS detects power attenuation and oscillation on the feeder connected to the main grid, indicating impending load shedding and supply interruption. At this point, it is necessary to immediately assess the risk of disconnection from the main grid and make the corresponding SR strategy, which consists of a set of tasks, including MEG allocation, defensive MG reconfiguration, and reserve commitment. It assumes that the power supply area of the main grid where the IEHS is located is interrupted due to a disaster. In the process of implementation, the MEG connects to the pre-positioned bus to supply power to the critical load, and the PDS is divided into multiple MGs, with all equipment operating according to the reserve plan.

The IEHS remains in the fault area, and the continuous impact of extreme events can cause secondary strikes within the IEHS, introducing uncertainty into the implementation process of the formulated SR strategy. To address this problem, we propose a two-stages tri-level problem based on the DRO model, as shown in Eq.(1), to enhance the robustness of the SR strategy. In the first stage, we describe the outer layer problem, which determines multiple optimal SR strategies for IEHS. The second stage integrates middle layer and inner layer problem, exploring the worst-case distribution realization of secondary strikes by maximizing the optimal value of the inner layer problem. The probability distribution $\mathbb{P}$ of secondary strikes on the IEHS is assumed to be uncertain and operates within the ambiguity set $\mathcal{W}(\hat{\mathbb{P}},\mathcal{D}_w)$ constructed using historical data. The worst-case probability distribution searched is added to the first stage through the expectation operator of the value function $\mathcal{Q}(\boldsymbol{x}, \boldsymbol{i}, \boldsymbol{\xi})$. The inner problem seeks the optimal SR implementation to minimize penalties from the unplanned power and thermal loads shedding and wind power curtailment in response to the uncertainty secondary strikes. The robustness of the two stages tri-level problem solution is ensured by minimizing the total cost of the first stage under the worst-case probability distribution within the ambiguity set $\mathcal{W}(\hat{\mathbb{P}},\mathcal{D}_w)$, using "max-min" operators.

$$\begin{aligned} \min_{\boldsymbol{x}\in\mathcal{X},\boldsymbol{z}} \ & \boldsymbol{c}^{\mathrm{T}}\boldsymbol{x} + \max_{\mathbb{P}\in\mathcal{W}(\hat{\mathbb{P}},\theta)} E_{\mathbb{P}}\left[\mathcal{Q}(\boldsymbol{x},\boldsymbol{i},\boldsymbol{\xi})\right] \\ \text{s.t.} \ & \boldsymbol{A}\boldsymbol{x} + \boldsymbol{B}\boldsymbol{z} \le \boldsymbol{b} \\ & \boldsymbol{D}\boldsymbol{z} \le \boldsymbol{f} \\ & \boldsymbol{x} \in \mathbb{R}^{|\mathcal{X}|\times|T|}, \boldsymbol{z} \in \mathbb{B}^{|\mathcal{L}|\times|\mathcal{T}|} \end{aligned} \quad \boldsymbol{\xi}\in\Xi \tag{1}$$

In Eq.(1), $\boldsymbol{x}$ and $\boldsymbol{z}$ are continuous and binary variables of the SR strategy, which represent reserve, unit commitment and defensive MG reconfiguration respectively. $\boldsymbol{\xi}$ are the binary uncertain variables of the worst-case scenario. The E is the expectation operator, $\boldsymbol{A}$, $\boldsymbol{B}$, $\boldsymbol{D}$, $\boldsymbol{b}$ and $\boldsymbol{f}$ are constant matrices and their corresponding constraints.

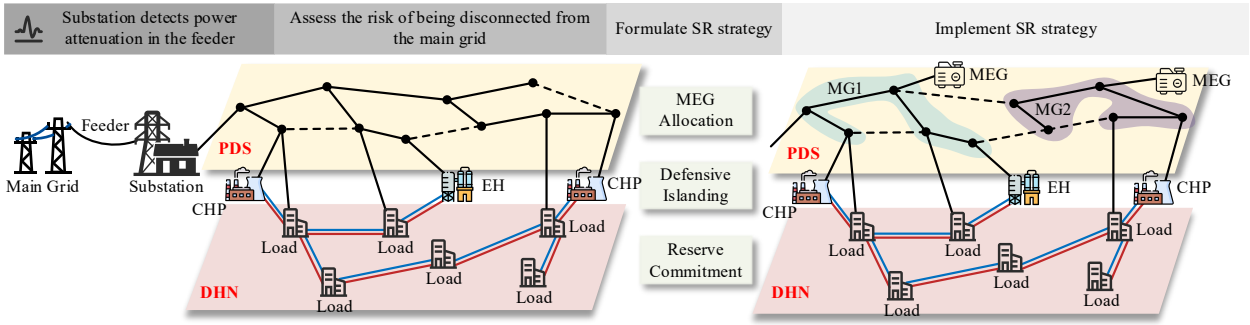

Fig. 1 Framework of SR strategy for IEHS

In the inner layer problem, we consider the continuous implementation of SR decisions within a scheduling period. We measure the total penalty of load shedding under defensive MG reconfiguration and MEG allocation $\boldsymbol{z}$, reserve decision $\boldsymbol{x}$ and subsequent uncertain fault $\boldsymbol{\xi}$ while SR is implemented. During the SR strategy operation, the IEHS can utilize the VES capacity in the DHN and the corrective dispatch within the reserve capacity to minimize the emergency load reduction, as shown in Eq.(2):

$$\begin{aligned} \mathcal{Q}(\boldsymbol{x},\boldsymbol{i},\boldsymbol{\xi}) = \min_{\boldsymbol{y}} \ & \boldsymbol{d}^{\mathrm{T}}\boldsymbol{y} \\ s.t. \ & \boldsymbol{E}\boldsymbol{x}+\boldsymbol{H}\boldsymbol{y}+\boldsymbol{N}\boldsymbol{i} \le \boldsymbol{r} \\ & \boldsymbol{y} \in \mathbb{R}^{|\mathcal{Y}|\times|T|}, \boldsymbol{i} \in \mathbb{B}^{|\mathcal{L}|\times|T|} \end{aligned} \tag{2}$$

where, $\boldsymbol{E}$, $\boldsymbol{H}$, $\boldsymbol{N}$ and $\boldsymbol{r}$ are constant matrices and their corresponding constraints. The variable $\boldsymbol{i}$ realizes the coupling of defensive MG reconfiguration and secondary strikes through AND operation. $\boldsymbol{y}$ is the decision variable to achieve the minimum load shedding penalty.

2.2 The VES of IEHS

We analyze the demand for electricity and thermal by users in the IEHS during the formulation and implementation of the SR strategy. The electricity demand is met by MEG, wind turbines (WT), and CHP units, while the thermal demand is supplied by CHP units and EH units. The CHP units burn natural gas to supply electricity and thermal simultaneously in a fixed ratio, while the EH units consume electricity to convert into thermal. Electricity and thermal are distributed to consumers through the PDS and the DHN, respectively.

In the heating distribution system, the DHN benefits from the presence of flexible energy storage capacity due to its inherent thermal inertia, thereby enhancing system flexibility on the IEHS. We introduce the concept of VES to describe the high-capacity energy storage characteristics exhibited by the DHN. Unlike traditional thermal energy storage systems, VES does not have device parameters such as state of charge, charge/discharge thermal energy, or charge/discharge thermal efficiency. Although some scholars model VES as a thermal energy storage device [32], this is only a mathematical equivalence and does not accurately reflect the actual characteristics of the DHN.

We developed a model considering the transmission delay in the DHN based on its quasi-steady-state model [31]. In each scheduling interval Δt, we assume that a mass block flows through the pipeline p from the inlet to the outlet, with the time taken recorded as τ_p. This time may not necessarily be an integer multiple of the scheduling interval Δt. Therefore, we use the weighted average of the temperatures of the two mass blocks at the outlet, denoted as $\tau_1=(K\text{-}1)\Delta t$ and $\tau_2=K\Delta t$. By calculation, the temperature at the pipeline outlet can be determined as:

$$\begin{aligned} T_{p,t}^{\mathrm{s/r,out}} &= \frac{q_K(\tau_2-\tau_p)T_{K,p,t}^{\mathrm{s/r,out}} + q_{K+1}(\tau_p-\tau_1)T_{K+1,p,t}^{\mathrm{s/r,out}}}{q_K(\tau_2-\tau_p)+q_{K+1}(\tau_p-\tau_1)} \\ &= C_1 T_{K,p,t}^{\mathrm{s/r,out}} + C_2 T_{K+1,p,t}^{\mathrm{s/r,out}} \end{aligned} \quad \forall p\in\mathcal{P}, \forall t\in\mathcal{T} \tag{3}$$

where, C_1 and C_2 are the weighting coefficients of $T_{K,p,t}^{\mathrm{s/r,out}}$ and $T_{K+1,p,t}^{\mathrm{s/r,out}}$ respectively.

During the thermal transmission process in the DHN, thermal exchange with the external environment leads to a decrease in temperature at the pipeline outlet compared to the inlet. Incorporating this with the quasi-steady-state Eq.(3) of the DHN, we can express the temporal coupling constraints of the temperatures at the pipeline inlet and outlet as:

$$\begin{cases} T_{p,t}^{\mathrm{s/r,out}} = C_1C_3T_{p,t-\tau_1}^{\mathrm{s/r,in}} + C_2C_4T_{p,\tau_2-t}^{\mathrm{s/r,in}} + (1-C_1C_3-C_2C_4)T_t^{\mathrm{A}} \\ C_3 = e^{-a_K L_p}, C_4 = e^{-a_{K+1}L_p}, a_K = k_p/(q_K c^{\mathrm{P}}) \end{cases} \quad \forall p\in\mathcal{P}, \forall t\in\mathcal{T} \tag{4}$$

In Eq.(4), we observe that under the mass flow control mode, the temperature at the pipe outlet can be represented as a linear combination of inlet temperatures at various scheduling times. Here, C_3 and C_4 serve as auxiliary coefficients in the linear formulation.

2.3 Construction of Ambiguity Set and Support Set

In this subsection, the uncertainties of secondary strikes to the branch are described by an ambiguity set that contains the true distribution function with a specified Wasserstein distance and a given discrete support set.

2.3.1 Ambiguity set

The ambiguity set is constructed using a data-driven approach that does not rely on a specific distribution. It characterizes the entire distribution within the probability space, centered on the empirical distribution and constrained by the Wasserstein distance metric. We utilize $\mathcal{D}_w$ represents the Wasserstein distance between the real distribution $\mathbb{P}$ and the empirical distribution $\hat{\mathbb{P}}$:

$$\begin{aligned} \mathcal{D}_w(\mathbb{P},\hat{\mathbb{P}}) &= \inf_{\Pi}\left\{E_{\Pi}\left[d(\boldsymbol{\xi},\hat{\boldsymbol{\xi}})\right]: \boldsymbol{\xi}\sim\mathbb{P}, \hat{\boldsymbol{\xi}}\sim\hat{\mathbb{P}}\right\} \\ &= \inf_{\Pi\in P(\Xi\times\Xi)} \int_{\boldsymbol{\xi}\in\Xi}\int_{\hat{\boldsymbol{\xi}}\in\Xi} \left\|\boldsymbol{\xi}-\hat{\boldsymbol{\xi}}\right\|^p \Pi\, d\hat{\boldsymbol{\xi}}\, d\boldsymbol{\xi} \end{aligned} \tag{5}$$

where, $\|\cdot\|^p$ represent the p norm operations are used to calculate the distance between two random vectors. The empirical distribution is defined as an estimate of the distribution of historical data $\hat{\mathbb{P}} = \sum_s p_s \delta(\hat{\boldsymbol{\xi}}^s)$, where, $\delta()$ represents the Dirac measure of sth sample.

It can be revealed from Eq.(5) that integrating the joint distributions results in an infinite optimization problem, making it difficult to tackle and requiring further processing. By leveraging the conditional distribution interpretation of $\Pi=\sum_{s=1}^{Ns} p_s \mathbb{P}_s$, the problem can be converted to utilize conditional distribution $\mathbb{P}_s$ as variables. Thus Eq.(5) can be written as a semi-infinite optimization as shown in Eq.(6):

$$\mathcal{D}_w(\mathbb{P},\hat{\mathbb{P}}) = \inf_{\mathbb{P}_s>0} \sum_{s=1}^{Ns} \int_{\boldsymbol{\xi}\in\Xi} p_s \left\|\boldsymbol{\xi}-\hat{\boldsymbol{\xi}}\right\|^p \mathbb{P}_s\, d\boldsymbol{\xi} \tag{6}$$

The ambiguity set $\mathcal{W}(\hat{\mathbb{P}},\theta)$ is defined by two parameters $\hat{\mathbb{P}}$ and θ:

$$\mathcal{W}(\hat{\mathbb{P}},\theta) = \left\{\mathbb{P}\in P(\Xi) \middle| \mathcal{D}_w(\mathbb{P},\hat{\mathbb{P}}) \le \theta\right\} \tag{7}$$

The ambiguity set is centered on the empirical distribution $\hat{\mathbb{P}}$ and is defined within a radius θ measured by the Wasserstein distance. This set encompasses all probability measures supported by the random variables $\boldsymbol{\xi}$ on the corresponding support set Ξ. The conservatism of the solution can be controlled by adjusting the size of θ. As the number of selected samples Ns increases, the empirical distribution will eventually converge to the true distribution, causing θ to approach zero. At a given confidence level, the empirical distribution is typically chosen to converge to the true distribution at an exponential rate [43], as demonstrated in formulation Eq.(8):

$$P\left(\mathcal{D}_w(\mathbb{P},\hat{\mathbb{P}}) \le \theta\right) \ge 1-\exp\left(-Ns\frac{\theta^2}{C^2}\right) \tag{8}$$

Therefore, θ can be represented by a given confidence level γ:

$$\theta = C\sqrt{\frac{1}{Ns}\ln\left(\frac{1}{1-\gamma}\right)} \tag{9}$$

In Eq.(9), C is a constant, which can be obtained by solving the following problem Eq.(10):

$$C=\min_{\omega>0}\sqrt{\frac{2}{\omega}\left\{1+\ln\left[\sum_{s}p_s\exp\left(\omega\left\|\hat{\xi}-\bar{\xi}\right\|^2\right)\right]\right\}} \tag{10}$$

where, $\bar{\xi}$ is the mean of $\hat{\boldsymbol{\xi}}$.

2.3.2 Support set

A fundamental component of DRO is the support set, which defines the range of values for random variables. In this paper, the support set defines the binary status of branch *l* during the SR implementation process, where 0 indicates that the branch was attacked by a secondary strike and has left the system, while 1 indicates that it remains in the system. The random variables are distributed within the $\mathcal{D}_w$ probability space and are constrained by the box support set Ξ, as shown in Eq.(11).

$$\Xi=\left\{\boldsymbol{\xi}\in\mathbb{R}^{|\mathcal{L}|\times|\mathcal{T}|}\left|\begin{array}{l}\sum_{l}\xi_{l,t}\geq|\mathcal{L}|-k,\xi_{l,\tau}\leq\xi_{l,t}\quad\forall\tau>t\\ \sum_{t}\sum_{l}\xi_{l,t}\leq\Gamma\end{array}\right.\right\} \tag{11}$$

In this support set, the first line of Eq.(11) specifies that *N-k* branches remain undamaged after secondary strikes, where *k* is limited by the maximum number of simultaneously faulty branches in the historical dataset $\hat{\boldsymbol{\xi}}$. Additionally, the support set mandates that faulty branches remain disconnected until the end of the SR implementation process. The conservative parameter Γ, introduced in the second line of Eq.(11), limits the total disconnection time of the faulty branches to control the severity of secondary strikes.

3. Mathematical Formulation

3.1 MEG Allocation and Defensive MG Reconfiguration

3.1.1 MEG allocation

MEGs can control the access electricity bus to provide power and maintain voltage stability in the MG. We utilize MEGs as the root bus of the MG and perform defensive MG reconfiguration operations based on them. During the SR formulation process, MEGs are deployed on the appropriate bus of the PDS and maintain appropriate hot reserve or cold reserve status. After realizing that the IEHS is disconnected from the main grid, they are connected to the pre-positioned bus and maintain the voltage stability of the self-organizing MG. In the SR strategy formulation problem, the constraints on MEG allocation are as follows:

$$\sum_{g\in\mathcal{G}}A_{i,g}^{\mathrm{MEG}}\leq 1,\quad\forall i\in\mathcal{B} \tag{12}$$

$$\sum_{i\in\mathcal{B}}A_{i,g}^{\mathrm{MEG}}=1,\quad\forall g\in\mathcal{G} \tag{13}$$

$$\sum_{i\in\mathcal{B}}\sum_{g\in\mathcal{G}}A_{i,g}^{\mathrm{MEG}}\leq N^{\mathrm{MEG}},\quad\forall i\in\mathcal{B},\forall g\in\mathcal{G} \tag{14}$$

Eq.(12) and (13) ensure that MEGs can only be assigned to a single bus, while Eq.(14) ensures that the total number of buses assigned to MEGs does not exceed the total number of MEG units available.

3.1.2 Defensive MG reconfiguration logic constraints

Eq.(15) and (16) ensure that buses are assigned to their respective MG, which must have a root bus to be operational. For a branch to be part of MG *m*, both bus *i* and bus *j* at its ends must belong to MG *m*, as captured by Eq.(17). If bus *i* and bus *j* belong to different MGs, Eq.(18) restricts that switch Sw_l disables branch *l* connecting them.

$$\sum_{m\in\mathcal{M}}x_{i,m}=1,\quad\forall i\in\mathcal{B} \tag{15}$$

$$x_{i,m}\leq x_{r_m,m},\quad\forall i\in\mathcal{B},\forall m\in\mathcal{M} \tag{16}$$

$$y_{l,m}=x_{i,m}x_{j,m},\quad\forall i,j\in\mathcal{B},\forall l\in\mathcal{L},\forall m\in\mathcal{M} \tag{17}$$

$$\sum_{m\in\mathcal{M}}y_{l,m}=Sw_l,\quad\forall l\in\mathcal{L},\forall m\in\mathcal{M} \tag{18}$$

3.1.3 MG radial constraints

PDS is typically constructed in a mesh structure but needs to operate in a radial configuration to coordinate the relay protection scheme, which is fundamental for defensive MG reconfiguration. The realization of a radial network within the MG relies on satisfying two conditions [44]. *Condition 1* is captured by Eq.(19), which mandates equality between bus-branch discrepancies and root bus quantities. *Condition 2* emphasizes maintaining connectivity within MGs, elucidated further in the connectivity constraints.

$$\sum_{m\in\mathcal{M}}\sum_{i\in\mathcal{N}}x_{i,m}-\sum_{m\in\mathcal{M}}\sum_{l\in\mathcal{L}}y_{l,m}=\sum_{m\in\mathcal{M}}x_{r_m,m} \tag{19}$$

3.1.4 MG connectivity constraints

Both single-commodity flow and multi-commodity flow can constrain the connectivity of MG. Here, commodity refers to products moving between sources and sinks, serving as a virtual representation of network connections, also known as fictitious flow [7]. The specifies commodity are exclusively generated at the root node, captured by Eq.(20), while Eq.(21) denotes that each connected node within MG *m* functions as a sink with a capacity of 1/|$\mathcal{N}$|. Additionally, Eq.(22) restricts commodity flow to paths existing between buses within MG *m* and the root bus.

$$0\leq g_{r_m}\leq x_{r_m,m},\quad\forall m\in\mathcal{M} \tag{20}$$

$$\sum_{i\in to(ji)|ji\in\mathcal{L}}f_{ji}-\sum_{i\in fr(ji)|ik\in\mathcal{L}}f_{ik}+g_i=1/|\mathcal{N}|\sum_{m\in\mathcal{M}}x_{i,m},\quad\forall i\in\mathcal{N} \tag{21}$$

$$-\sum_{m\in\mathcal{M}}y_{l,m}\leq f_l\leq\sum_{m\in\mathcal{M}}y_{l,m},\quad\forall l\in\mathcal{L} \tag{22}$$

3.2 Outer layer Problem

The objective function of the SR strategy formulation outer layer problem is shown in Eq.(23), which aims to the minimum SR investment. This includes the total cost of providing energy reserve and configuring the start-shut state of units:

$$\min\sum_{t\in T}\left(\begin{array}{l}\sum_{c\in\mathcal{C}}c_c^{suc}u_{c,t}+c_c^{sdc}v_{c,t}+c_c^{onc}i_{c,t}+\rho_c^{\mathrm{CHP}}\left(\bar{P}_{c,t}^{\mathrm{CHP}}-\underline{P}_{c,t}^{\mathrm{CHP}}\right)+\\ \sum_{h\in\mathcal{H}}\rho_h^{\mathrm{EH}}\left(\bar{P}_{h,t}^{\mathrm{EH}}-\underline{P}_{h,t}^{\mathrm{EH}}\right)+\sum_{g\in\mathcal{G}}\rho_g^{\mathrm{MEG}}\left(\bar{P}_{g,t}^{\mathrm{MEG}}-\underline{P}_{g,t}^{\mathrm{MEG}}\right)\end{array}\right) \tag{23}$$

In the specific formulation of the SR strategy, the minimum start-up/shut down requirements of CHP and MEG are expressed as follow:

$$u_{b,t}-v_{b,t}=i_{b,t}-i_{b,t-1},\quad\forall b\in\mathcal{C}\cup\mathcal{G},\forall t\in\mathcal{T} \tag{24}$$

$$u_{b,t}+v_{b,t}\leq 1,\quad\forall b\in\mathcal{C}\cup\mathcal{G},\forall t\in\mathcal{T} \tag{25}$$

$$\left(i_{b,t+1}-i_{b,t}\right)T_b^{\mathrm{on}}-\sum_{k=t+2}^{\min\left\{t+T_b^{\mathrm{on}},|\mathcal{T}|\right\}}i_{b,k}\leq\max\left\{1,T_b^{\mathrm{on}}-|\mathcal{T}|+t-1\right\},\quad\forall b\in\mathcal{C}\cup\mathcal{G},\forall t\in\mathcal{T} \tag{26}$$

$$\left(i_{b,t}-i_{b,t+1}\right)T_b^{\mathrm{off}}-\sum_{k=t+2}^{\min\left\{t+T_b^{\mathrm{off}},|\mathcal{T}|\right\}}i_{b,k}\leq T_b^{\mathrm{off}},\quad\forall b\in\mathcal{C}\cup\mathcal{G},\forall t\in\mathcal{T} \tag{27}$$

In the SR strategy formulation outer layer problem, we propose a reserve formulation. This reserve dispatch plan ensures that the unit has sufficient ramping ability in adjacent time intervals to achieve decoupling in

operating time. Additionally, the unit's output is covered in the reserve interval, which helps reduce the unit status indicator variables during the optimization problem-solving process, thereby avoiding the increase in computational complexity caused by processing these indicator variables [45]. The ramping limits for CHP reserve boundaries are as following:

$$\bar{P}_{c,t}^{\mathrm{CHP}} - \underline{P}_{c,t-1}^{\mathrm{CHP}} \le RU_c^{\mathrm{CHP}} \cdot i_{c,t-1} + P_{c,\max}^{\mathrm{CHP}} \cdot \left(1 - i_{c,t-1}\right), \quad \forall c \in \mathcal{C}, \forall t \in \mathcal{T} \tag{28}$$

$$\bar{P}_{c,t-1}^{\mathrm{CHP}} - \underline{P}_{c,t}^{\mathrm{CHP}} \le RD_c^{\mathrm{CHP}} \cdot i_{c,t} + P_{c,\max}^{\mathrm{CHP}} \cdot \left(1 - i_{c,t}\right), \quad \forall c \in \mathcal{C}, \forall t \in \mathcal{T} \tag{29}$$

$$P_{c,\min}^{\mathrm{CHP}} i_{c,t} \le \underline{P}_{c,t}^{\mathrm{CHP}} \le \bar{P}_{c,t}^{\mathrm{CHP}} \le P_{c,\max}^{\mathrm{CHP}} i_{c,t}, \quad \forall c \in \mathcal{C}, \forall t \in \mathcal{T} \tag{30}$$

The ramping limits for EH reserve boundaries are as following:

$$\bar{P}_{h,t}^{\mathrm{EH}} - \underline{P}_{h,t-1}^{\mathrm{EH}} \le RU_h^{\mathrm{EH}}, \quad \forall h \in \mathcal{H}, \forall t \in \mathcal{T} \tag{31}$$

$$\bar{P}_{h,t-1}^{\mathrm{EH}} - \underline{P}_{h,t}^{\mathrm{EH}} \le RD_h^{\mathrm{EH}}, \quad \forall h \in \mathcal{H}, \forall t \in \mathcal{T} \tag{32}$$

$$P_{h,\min}^{\mathrm{EH}} \le \underline{P}_{h,t}^{\mathrm{EH}} \le \bar{P}_{h,t}^{\mathrm{EH}} \le P_{h,\max}^{\mathrm{EH}}, \quad \forall h \in \mathcal{H}, \forall t \in \mathcal{T} \tag{33}$$

And same to the MEG:

$$\bar{P}_{g,t}^{\mathrm{MEG}} - \underline{P}_{g,t-1}^{\mathrm{MEG}} \le RU_g^{\mathrm{MEG}}, \quad \forall g \in \mathcal{G}, \forall t \in \mathcal{T} \tag{34}$$

$$\bar{P}_{g,t-1}^{\mathrm{MEG}} - \underline{P}_{g,t}^{\mathrm{MEG}} \le RU_g^{\mathrm{MEG}}, \quad \forall g \in \mathcal{G}, \forall t \in \mathcal{T} \tag{35}$$

$$P_{g,\min}^{\mathrm{MEG}} \le \underline{P}_{g,t}^{\mathrm{MEG}} \le \bar{P}_{g,t}^{\mathrm{MEG}} \le P_{g,\max}^{\mathrm{MEG}}, \quad \forall g \in \mathcal{G}, \forall t \in \mathcal{T} \tag{36}$$

3.3 Inner layer Problem

As shown in Eq.(37), the objective function of the SR strategy implemented inner layer problem aims to minimize the operation cost, which consists of the unplanned shedding penalty of the power and thermal loads, the penalty of wind power curtailment, and the units adjusting cost. The objective function can be expressed as follows:

$$\min \sum_{t \in \mathcal{T}} \left(\begin{array}{l} \sum_{d \in D} C_d^{\mathrm{Loss}} \left(P_{d,t}^{\mathrm{Loss}} + Q_{d,t}^{\mathrm{Loss}} \right) + \sum_{n \in \mathcal{E}} C_n^{\mathrm{Loss}} H_{n,t}^{\mathrm{Loss}} + \sum_{w \in \mathcal{W}} C_w^{\mathrm{cur}} \left(A_{w,t}^{\mathrm{WT}} - P_{w,t}^{\mathrm{WT}} \right) \\ \sum_{c \in \mathcal{C}} f_c^{\mathrm{CHP}} \left(P_c^{\mathrm{CHP}}, H_c^{\mathrm{CHP}} \right) + \sum_{g \in \mathcal{G}} C_g^{\mathrm{MEG}} P_g^{\mathrm{CHP}} + \sum_{h \in \mathcal{H}} C_h^{\mathrm{EH}} P_h^{\mathrm{EH}} \end{array} \right) \tag{37}$$

where, f_c^{CHP} is the fuel cost function of CHP units.

3.3.1 Dispatch constraints

During the process of SR strategy implementation, units can redistribute power according to the reserve intervals scheduled in the formulated plan, and WT can operate to obtain power within the available wind power capacity. The constraints are as follows:

$$\underline{P}_{c,t}^{\mathrm{CHP}} \le P_{c,t}^{\mathrm{CHP}} \le \bar{P}_{c,t}^{\mathrm{CHP}}, \quad \forall c \in \mathcal{C}, \forall t \in \mathcal{T} \tag{38}$$

$$\underline{P}_{h,t}^{\mathrm{EH}} \le P_{h,t}^{\mathrm{EH}} \le \bar{P}_{h,t}^{\mathrm{EH}}, \quad \forall h \in \mathcal{H}, \forall t \in \mathcal{T} \tag{39}$$

$$\underline{P}_{g,t}^{\mathrm{MEG}} \le P_{g,t}^{\mathrm{MEG}} \le \bar{P}_{g,t}^{\mathrm{MEG}}, \quad \forall g \in \mathcal{G}, \forall t \in \mathcal{T} \tag{40}$$

$$0 \le P_{w,t}^{\mathrm{WT}} \le A_{w,t}^{\mathrm{WT}}, \quad \forall w \in \mathcal{W}, \forall t \in \mathcal{T} \tag{41}$$

3.3.2 PDS constraints

Since the radial topology is guaranteed during the defensive MG reconfiguration process, the DistFlow branch model is utilized to describe power flow constraints. The active power and reactive power decomposition form combines the reactive power and voltage amplitude, which is more suitable for description in the PDS than the DC form due to its power balance and power flow equation, and transmission branch restrictions.

$$\begin{aligned} &\sum_{c \in \mathcal{C}} P_{c,t}^{\mathrm{CHP}} + \sum_{g \in \mathcal{G}} A_{i,g}^{\mathrm{MEG}} P_{g,t}^{\mathrm{MEG}} + \sum_{w \in \mathcal{W}} P_{w,t}^{\mathrm{WT}} + \sum_{i \in to(ji) | ji \in \mathcal{L}} Pf_{ji,t} = \\ &\qquad \sum_{i \in fr(ik) | ik \in \mathcal{L}} Pf_{ik,t} + \sum_{h \in \mathcal{H}} P_{h,t}^{\mathrm{EH}} + \sum_{d \in D} \left(P_{d,t}^{\mathrm{L}} - P_{d,t}^{\mathrm{Loss}} \right) \end{aligned} \quad \forall i \in \mathcal{B}, \forall t \in \mathcal{T} \tag{42}$$

$$\begin{aligned} &\sum_{c \in \mathcal{C}} Q_{c,t}^{\mathrm{CHP}} + \sum_{g \in \mathcal{G}} A_{i,g}^{\mathrm{MEG}} Q_{g,t}^{\mathrm{MEG}} + \sum_{i \in to(ji) | ji \in \mathcal{L}} Qf_{ji,t} = \\ &\qquad \sum_{i \in fr(ik) | ik \in \mathcal{L}} Qf_{ik,t} + \sum_{d \in D} \left(Q_{d,t}^{\mathrm{L}} - Q_{d,t}^{\mathrm{Loss}} \right) \end{aligned} \quad \forall t \in \mathcal{T} \tag{43}$$

$$-\overline{Pf}_l \cdot z_{l,t} \le Pf_{l,t} \le \overline{Pf}_l \cdot z_{l,t}, \quad \forall l \in \mathcal{L}, \forall t \in \mathcal{T} \tag{44}$$

$$-\overline{Qf}_l \cdot z_{l,t} \le Qf_{l,t} \le \overline{Qf}_l \cdot z_{l,t}, \quad \forall l \in \mathcal{L}, \forall t \in \mathcal{T} \tag{45}$$

$$V_{fr(l),t} - \left(P_{l,t} r_l + Q_{l,t} x_l \right) / V - V_{to(l),t} \le M \left(1 - z_{l,t} \right), \quad \forall l \in \mathcal{L}, t \in \mathcal{T} \tag{46}$$

$$V_{fr(l),t} - \left(P_{l,t} r_l + Q_{l,t} x_l \right) / V - V_{to(l),t} \ge M \left(1 - z_{l,t} \right), \quad \forall l \in \mathcal{L}, t \in \mathcal{T} \tag{47}$$

$$\underline{V}_i \le V_{i,t} \le \bar{V}_i, \quad \forall i \in \mathcal{B}, \forall t \in \mathcal{T} \tag{48}$$

The operation of the PDS is constrained by Eq.(42)-Eq.(48). Eq.(42) and (43) ensure the active and reactive power balance at each bus. Eq.(44) and (45) enforce that there is no active or reactive power flow on the damaged or open branch. Eq.(46) and (47) represent the relationship between voltage amplitude and branch flow, which are decoupled using the big-M method for the damaged or open branches. Eq.(48) limits the boundary conditions that the voltage amplitude on the connected bus needs to meet.

3.3.3 DHN constraints

We assume that the DHN operates in constant flow and variable temperature (CF-VT) control mode. This mode changes the temperature of the heating network working fluid while keeping the mass flow rate constant, taking thermal inertia into consideration. The following equations, together with Eq.(3) and (4), constitute the DHN supply and return water pipeline model under the CF-VT mode:

$$\sum_{c \in \mathcal{C}} H_{c,t}^{\mathrm{CHP}} + \sum_{h \in \mathcal{H}} H_{h,t}^{\mathrm{EH}} = c^{\mathrm{P}} m_{n,t} \left(T_{n,t}^{\mathrm{s}} - T_{n,t}^{\mathrm{r}} \right), \quad \forall n \in \mathcal{S}, t \in \mathcal{T} \tag{49}$$

$$H_{n,t}^{\mathrm{L}} - H_{n,t}^{\mathrm{Loss}} = c^{\mathrm{P}} m_{n,t} \left(T_{n,t}^{\mathrm{s}} - T_{n,t}^{\mathrm{r}} \right), \quad \forall n \in \mathcal{E}, \forall t \in \mathcal{T} \tag{50}$$

$$\sum_{p \in \mathcal{P}} \left(m_{p,t}^{\mathrm{s/r}} T_{p,t}^{\mathrm{s/r,out}} \right) = T_{n,t}^{\mathrm{s/r,mix}} \sum_{p \in \mathcal{P}} m_{p,t}^{\mathrm{s/r}}, \quad \forall n \in \mathcal{N}, \forall t \in \mathcal{T} \tag{51}$$

$$T_{n,t}^{\mathrm{s/r,mix}} = T_{p,t}^{\mathrm{s/r,in}}, \quad \forall n \in \mathcal{N}, \forall p \in \mathcal{P}, \forall t \in \mathcal{T} \tag{52}$$

Eq.(49) and (50) represent the exchange of thermal energy at the thermal source and thermal load, respectively. Eq.(51) and (52) represent the exchange of thermal energy in the DHN pipeline. Specifically, Eq.(51) represents the constraint of temperature mixing at the outlet of the pipeline, and Eq.(52) states that the temperature at the inlet of the pipeline is the same as the temperature at the mixing point of the pipeline.

4. Solution Methodology

4.1 Logical constraints convex relaxation

4.1.1 AND logical constraints linearization

In the SR strategy implemented inner layer problem, the branch operation status is simultaneously influenced by the SR strategy result $\boldsymbol{z}$ and the subsequent fault $\boldsymbol{\xi}$ under the worst-case distribution**,** which is constrained by the AND operator. The multiplication of the two binary variables can be converted into the following constraints:

$$\begin{cases} \boldsymbol{i}_S \le \boldsymbol{z} \\ \boldsymbol{i}_S \le \boldsymbol{\xi}_S \\ \boldsymbol{i}_S \ge \boldsymbol{z} + \boldsymbol{\xi}_S - 1 \end{cases} \tag{53}$$

4.1.2 If constraint linearization

In the process of organizing the MG, the root node of the MG must first be determined, as shown in Eq.(20). Simultaneously, the deployment of the MEG as an optimization variable needs to be addressed during the MG defensive decision-making stage, thereby forming an *If* constraint problem, as shown in the following:

$$\boldsymbol{\Delta}^{-} = \begin{cases} 1, \ if \ g_{r_m} \ge 0 \\ 0, \ else \end{cases} \tag{54}$$

$$\boldsymbol{\Delta}^{+}=\begin{cases}1, \ if \ x_{r_m,m}-g_{r_m}\geq 0\\ 0, \ else\end{cases} \tag{55}$$

By introducing auxiliary binary variables $\boldsymbol{\Delta}^{-}$ and $\boldsymbol{\Delta}^{+}$ we can indicate whether bus i is a potential feasible root bus. For the linearization of the *If-else* conditional expression, a sufficiently small positive constant ϵ and a sufficiently large constant M are utilized. Taking constraint (55) as an example:

$$\begin{cases}x_{r_m,m}-g_{r_m}+\epsilon\leq M\boldsymbol{\Delta}^{+}\\ x_{r_m,m}-g_{r_m}\geq M\left(\boldsymbol{\Delta}^{+}-1\right)\end{cases} \tag{56}$$

This formulation ensures that the potential root bus i is correctly identified and managed within the optimization framework, allowing the MEG unit to effectively serve as the root node of the MG under the specified conditions. Finally, the decision results of the auxiliary variables can be unified through the AND constraint, $\boldsymbol{\Delta}=\boldsymbol{\Delta}^{-}\&\boldsymbol{\Delta}^{+}$, The linearization process of this AND constraint is similar to that of Eq.(53).

4.2 Reformulation of DRO Model

The DRO model, represented by Eq.(1), is a mixed integer linear programming problem composed of the SR strategy formulation outer layer problem and the SR strategy implemented inner layer problem under infinite-dimensional support. Full support of the ambiguity set with infinite support is crucial for precise and robust decisions. However, there are infinite distributions within the empirical distribution Wasserstein metric $\mathcal{D}_w$, leading to an infinite number of recourse problems to identify the worst-case distribution. This high complexity makes solving the original DRO model challenging. Therefore, we adopt the conditional distribution expressed in Eq.(6) and reconstruct the expected expressing of Eq.(1) into the following form by employing the duality theory of infinite-dimensional optimization problems:

$$\begin{aligned}&\max_{\mathbb{P}\in\mathcal{W}(\hat{\mathbb{P}},\theta)} E_{\mathbb{P}}\left[\mathcal{Q}(\boldsymbol{x},\boldsymbol{i},\boldsymbol{\xi})\right]=\max_{\mathbb{P}_s}\sum_{s=1}^{Ns}\int_{\boldsymbol{\xi}\in\Xi}p_s\mathcal{Q}(\boldsymbol{x},\boldsymbol{i},\boldsymbol{\xi})\mathbb{P}_s d\boldsymbol{\xi}\\ &s.t.\ \ \int_{\boldsymbol{\xi}\in\Xi}\mathbb{P}_s d\boldsymbol{\xi}=1 \quad :\alpha_s\\ &\quad\sum_{s=1}^{Ns}\int_{\boldsymbol{\xi}\in\Xi}p_s\left\|\boldsymbol{\xi}-\hat{\boldsymbol{\xi}}\right\|^{p}\mathbb{P}_s d\boldsymbol{\xi}\leq\theta \quad :\beta\end{aligned} \tag{57}$$

where, α_s and β are dual variables.

The second line of Eq.(57) indicates that the integral of $\mathbb{P}_s$ is 1, ensuring that $\mathbb{P}_s$ is a valid distribution. The third line ensures that all distributions within a Wasserstein distance of θ from the empirical distribution are included in the ambiguity set, measured by the L_p-norm Wasserstein metric.

For problems described in Eq.(57), there exists at least one feasible solution, which is a relative interior point $\mathbb{P}_s=p_s\delta(\hat{\boldsymbol{\xi}}^s)$. Therefore, *Slater's* condition and strong duality hold. We can consider a semi-infinite optimization similar to the standard *Lagrange* duality in convex optimization allowing the problem can be reformulated as the dual formulation:

$$\begin{aligned}&\min_{\beta\geq 0,\alpha_s}\ \sum_{s=1}^{Ns}p_s\alpha_s+\beta\theta\\ &s.t.\ \ \mathcal{Q}(\boldsymbol{x},\boldsymbol{i},\boldsymbol{\xi})-\alpha_s-\beta\left\|\boldsymbol{\xi}-\hat{\boldsymbol{\xi}}\right\|^{p}\leq 0,\quad\forall\boldsymbol{\xi}\in\Xi,\forall s=1,\ldots,Ns\end{aligned} \tag{58}$$

According to the optimality condition, for the sth scenario, the optimal solution α_s under the worst-case distribution is as following:

$$\alpha_s=\max_{\boldsymbol{\xi}\in\Xi}\left\{\mathcal{Q}\left(\boldsymbol{x},\boldsymbol{i},\boldsymbol{\xi}^s\right)-\beta\left\|\boldsymbol{\xi}-\hat{\boldsymbol{\xi}}^s\right\|^{p}\right\} \tag{59}$$

The expectation of the worst-case $\max E_{\mathbb{P}}[\mathcal{Q}(\boldsymbol{x},\boldsymbol{i},\boldsymbol{\xi})]$ is equivalent to (60):

$$\min_{\beta\geq 0}\left\{\beta\theta+\sum_{s=1}^{Ns}p_s\max_{\boldsymbol{\xi}\in\Xi}\left[\mathcal{Q}\left(\boldsymbol{x},\boldsymbol{i},\boldsymbol{\xi}^s\right)-\beta\left\|\boldsymbol{\xi}-\hat{\boldsymbol{\xi}}^s\right\|^{p}\right]\right\} \tag{60}$$

Combined with the outer layer problem decisions, the DRO model, after reformulation, can be obtained. This combined model involves formulating SR strategy to adapt to a range of possible future scenarios under the worst-case distribution. In the outer layer problem, the model allows for independent SR strategy decisions to be made in preparation for potential secondary strikes. In the inner layer problem, given these initial decisions, the focus shifts to solving key scenarios to identify the worst-case distribution, thus constraining the outer layer problem decisions through recourse. Therefore, the reformulation implements a two-step process: 1) Simplification: by concentrating on a limited number of scenarios, the problem's complexity is reduced, making the outer layer decisions more manageable. 2) Robustness: by addressing key scenarios in the inner layer problem, we ensure that the decisions remain robust against the worst-case distribution within the Wasserstein metric.

The reconstructed DRO model resembles the classic two-stage RO. If the support set is convex and the Wasserstein distance is defined as L_1-norm or L_∞-norm, then problem Eq.(60) can be further expressed as a linear program. This linear program can be efficiently solved using decomposition algorithms, such as Benders and C&CG which alternate between two master-subproblems to guide the solution towards convergence.

4.3 Improved C&CG approach

The reformulated DRO model can be regarded as a variant of the conventional two-stage RO model. However, obtaining the worst-case probability distribution necessitates solving *Ns* subproblems. To avoid introducing norm expressions during the subproblem solving and the incorporation of cut hyperplanes involving norm operations into the master problem, thereby increasing the computational burden, the auxiliary variable κ_s is introduced into the C&CG iteration process [41], with detailed derivation provided in the Appendix. After solving the master problem, the solutions of the subproblems are influenced not only by the first-stage decision variables but also by the dual variable β and the auxiliary variable κ_s. Furthermore, during the process of adding C&CG cutting hyperplanes, it is essential to introduce convex relaxed logical constraints to reduce the solution space.

Step 1: Initialization. Set the convergence tolerance ε. Set the lower bound *LB* to -∞, the upper bound *UB* to +∞, and initialize the number of iterations c=1.

Step 2: Solve the following master problem:

$$\begin{aligned}&\min_{\boldsymbol{x}\in\mathcal{X},\boldsymbol{z},\alpha_s,\beta\geq 0,\kappa_s,\boldsymbol{y}_{c,s}}\ \boldsymbol{c}^{\mathrm{T}}\boldsymbol{x}+\sum_{s=1}^{Ns}p_s\alpha_s+\beta\theta\\ &s.t.\ \ \boldsymbol{A}\boldsymbol{x}+\boldsymbol{B}\boldsymbol{z}\leq\boldsymbol{b}\\ &\quad\boldsymbol{D}\boldsymbol{z}\leq\boldsymbol{f}\\ &\quad\left\|\kappa_s\right\|_{*}^{p}\leq\beta\\ &\quad\alpha_s\geq\boldsymbol{d}^{\mathrm{T}}\boldsymbol{y}-\kappa_s^{\mathrm{T}}\left(\boldsymbol{\xi}_{k,s}^{*}-\hat{\boldsymbol{\xi}}^s\right)\quad\forall k<c,\forall s\\ &\quad\boldsymbol{i}_{k,s}=\boldsymbol{z}\ \&\ \boldsymbol{\xi}_{k,s}^{*},\quad\forall k<c,\forall s\\ &\quad\boldsymbol{E}\boldsymbol{x}+\boldsymbol{H}\boldsymbol{y}_{k,s}+\boldsymbol{N}\boldsymbol{i}_{k,s}\leq\boldsymbol{r},\quad\forall k<c,\forall s\end{aligned} \tag{61}$$

Record the optimal solution $\boldsymbol{x}^*$, $\boldsymbol{z}^*$, κ^* and objective value, and update *LB* as the objective value of master problem.

Step 3: In each subproblem, the objective function is to minimize the emergency load shedding penalty under master problem's decisions and the

worst-case scenario. Since each subproblem is a linear programming problem, and the feasibility is always maintained through emergency load reduction, strong duality can be applied to transform it into the following dual problem:

$$\begin{aligned} \max_{\boldsymbol{\mu}\le 0,\boldsymbol{\xi}} \ & \left(\boldsymbol{r}-\boldsymbol{E}\boldsymbol{x}^{*}-\boldsymbol{N}\boldsymbol{i}\right)^{\mathrm{T}}\boldsymbol{\mu}-\boldsymbol{\kappa}_{s}^{*\mathrm{T}}\left(\boldsymbol{\xi}-\hat{\boldsymbol{\xi}}^{s}\right) \\ s.t. \ & \boldsymbol{i}=z^{*}\ \&\ \boldsymbol{\xi} \\ & \boldsymbol{H}^{\mathrm{T}}\boldsymbol{\mu}=\boldsymbol{d} \\ & \boldsymbol{\xi}\in\Xi \end{aligned} \tag{62}$$

where, $\boldsymbol{\mu}$ is the dual variable of the original subproblem, where the bilinear terms $\boldsymbol{N}^{\mathrm{T}}\boldsymbol{i}^{\mathrm{T}}\boldsymbol{\mu}$ are represented as the product of binary and continuous variables. These can be strictly converted into multiple linear constraints using McCormick's envelope method. Since this conversion process is rigorous [46], the resulting solutions are consistent with the original constraints.

Record the optimal solution $\boldsymbol{\mu}^{*}$, $\boldsymbol{\xi}^{*}$ and the objective value Q_s of subproblem s, and update the $UB = \min(UB, \boldsymbol{c}^{\mathrm{T}}\boldsymbol{x}^{*}+\sum_s p_s Q_s+\beta\theta)$

Step 4: If $(UB\text{-}LB)/LB < \varepsilon$, save present result and terminate the iterating process, otherwise, update $\boldsymbol{\xi}^{*}$ and $c=c+1$, and return *Step 1*.

5. Case Study

5.1 Simulation setting

We tested our approach on the modified 6-bus and 6-node system (M6B6N) and the modified IEEE 33-bus and 32-node system (M33B32N). The specific parameter settings of the system are described in Section 5.2 and 5.3, respectively. In both M6B6N and M33B32N, we assume that the substation and feeder are disconnected from the main grid at 00:00 due to the first strike of the extreme event, and secondary strikes to the IEHS from subsequent random events are modeled as typical branch outage faults. The confidence level γ for the Wasserstein radius of the ambiguity set in DRO model is set to 95%. In the SR strategy, the time interval for each decision schedule is 1 hour. All test codes in this section are implemented and executed using the JuMP.jl toolkit in the Julia language and solved by Gurobi Optimizer 9.5.2. The allowable tolerance ε for the improved C&CG algorithm is set to 0.1%. All programs were executed on a personal computer with 5GHz 12th Gen Inter Core i5 CPU and 32GB RAM.

5.2 Modified 6-bus and 6-node system

Our proposed model was tested on M6B6N. The system consists of a WT, a CHP unit, and a EH unit. The detailed parameters of the M6B6N can be found in Table 2. Considering the scale of the test system and the sparsity of historical extreme events, the ambiguity set is constructed from 50 groups of subsequent branch outage samples, recording N-1 unexpected events. The reserve cost is set to 30% of the power generation cost, and the unexpected load shedding penalties for the 3rd, 2nd, and 1st priority loads are 2 times, 3 times, and 5 times the power generation cost, respectively.

Table 2
Parameters of 6-bus and 6-node system

Parameter	Value	Parameter	Value
RU_g^{MEG}, RD_g^{MEG}	$0.3P_{g,\max}^{\mathrm{MEG}}$	RU_h^{EH}, RD_h^{EH}	$0.3P_{h,\max}^{\mathrm{EH}}$
T_g^{on}, T_g^{off}	0h, 1h	$\overline{V}_i$, $\underline{V}_i$	1.05, 0.95
RU_c^{CHP}, RD_c^{CHP}	$0.25P_{c,\max}^{\mathrm{CHP}}$	Γ	20
T_c^{on}, T_c^{off}	2h, 3h		

To verify the efficiency and stability of our proposed improved C&CG algorithm, we conducted convergence tests. The results, as shown in Fig. 2, demonstrate that the algorithm successfully converges within an acceptable number of iterations, ensuring the robustness and reliability of the SR strategy under the DRO model.

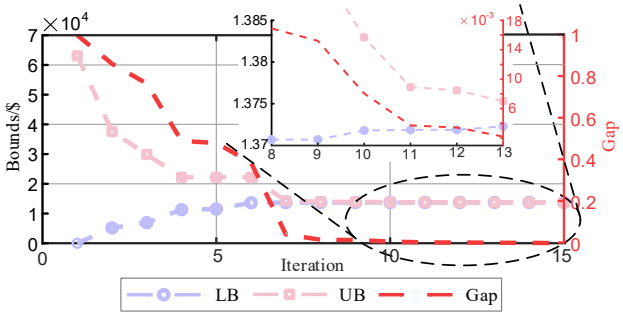

Fig. 2 The convergence of DRO model

The allocation of MEGs and the resulting defensive MG configurations are depicted in Fig. 3. This figure shows how MEGs are strategically deployed to critical buses and how the PDS is reconfigured into MGs to ensure a continuous power supply during extreme events.

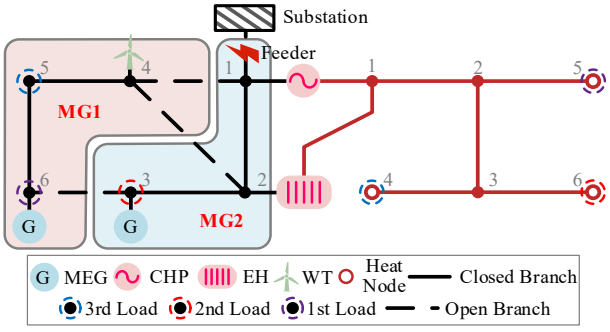

Fig. 3 The MEG allocation and defensive MG reconfiguration in M6B6N

MEGs can identify the load with the highest priority protection weight to ensure that load shedding occurs to the lowest extent during the SR implementation process. By utilizing the ability of MEGs to control bus voltage, ensuring stable voltage levels within the MG, which is crucial for maintaining the connectivity and allowing WT to be directly connected to the MG, we enhances the supply capacity of MG. Additionally, in the process of MEG allocation and defensive MG reconfiguration, the restriction that each bus in the MG is connected by a radial topology is observed.

5.2.1 Effectiveness of the DRO Model

To compare the performance of the DRO model proposed in this article, we first compare the results of the proposed DRO method with the results of three other model: the deterministic model, the SP model and the conventional two-stage RO model, which are marked as Case I, Case II, Case III and Case IV, respectively.

Case I: The basic model without considering specifical uncertainty, utilizing the mean of the historical data set as the boundary condition, overlooking the randomness of secondary strikes when formulating the SR strategy. In this scenario, the reserve commitment is set at 5% of the total load capacity.

Case II: The SP model, which decides the corresponding SR strategy using SP approach and is verified with the secondary strikes set constructed by historical data to obtain a more suitable scheduling.

Case III: The Conventional two-stage RO model characterizes secondary strikes utilizing a box uncertainty set, where the uncertainty set parameter Γ is selected based on the worst *N-k* faults identified in the historical data set.

Case IV: The proposed DRO model, which utilizes historical data set to construct the ambiguity set and support set to describe the uncertainty for secondary strikes in SR strategy formulation. (i.e., the proposed model)

Before presenting the application performance in different cases, we aim to illustrate that the proposed DRO model can achieve higher economic benefits and robustness, particularly through a more accurate estimation of secondary strikes. During the implementation of the SR strategy, out-of-sample tests are conducted to verify the performance of the proposed model and algorithm, which are sampled in 1000 possible secondary strikes scenarios by the Monte Carlo (MC) method to simulate a wide range of branch outage scenario. In the out-of-sample test, we compare the start/shut cost, reserve commitment cost, adjustment cost and average unexpected load shedding penalty cost across the four models (Case I-IV) in the MC simulating scenario, as shown in Table 3.

Table 3
Costs of Case I-IV under MC simulating scenario (10^4\$)

	Start/Shut	Reserve	Adjust	Avg.penalty	Total
Case I	2.5	0.84	1.90	25.52	30.76
Case II	2.5	1.15	2.36	9.33	15.34
Case III	3	1.22	2.82	8.75	15.79
Case IV	3	1.30	3.03	6.43	13.76

In terms of load shedding penalty costs, the performance order from best to worst is Case IV > Case II > Case III > Case I. The basic model in Case I formulates the SR solution purely from an economic perspective, aiming to minimize the formulation cost of the SR strategy. However, it incurs the highest unexpected load shedding penalty because MEG allocation, reserve commitment, and defensive MG reconfiguration ignore the uncertainty of secondary strikes, rendering the SR strategy ineffective under such circumstances.

Considering the uncertainty of secondary strikes, the total costs in Case II and Case III are significantly reduced compared to Case I, but the SP model (Case II) performs better than the conventional two-stage RO model (Case III). The two-stage RO model focuses only on the worst-case scenario, but the probability of these extreme scenarios occurring is very low. As a result, the SR strategy formulated by the conventional two-stage RO model fails to protect critical loads in many non-worst scenarios, leading to higher load shedding penalty costs.

Case II, using the SP model, considers multiple secondary strikes scenarios and adapts to various branch outage scenarios, resulting in better out-of-sample performance in most MC simulation samples. However, SP may lead to "overfitting," where the formulated SR strategy becomes ineffective if the actual strikes significantly deviate from the majority of scenarios considered.

In contrast, the DRO model (Case IV) utilizes the confidence level γ to construct an ambiguity set centered on the empirical distribution, incorporating the true probability distribution of secondary strikes at a specific confidence level. This ambiguity set also includes various potential distributions of secondary strikes event. This approach allows for the consideration of both worst-case and various non-worst-case scenarios in the formulation process of SR strategies. The worst secondary strike distribution is obtained by searching within the ambiguity set. The specific branch interruption events that may occur in each case within this worst distribution are constrained by the support set control parameter Γ in the DRO model, ensuring that the searched worst distribution has practical physical significance.

By combining ambiguity set with support set, the DRO-based SR strategy for IEHS achieves both economic efficiency (lower day-ahead SR strategy formulation cost) and robustness (lower unexpected load shedding penalty). Compared to the SP model, the DRO model emphasizes the probability information contained in the historical data set, searching for the worst-case distribution under the confidence level γ and the event combinations that conform to this distribution, resulting in a total operation cost reduction of 10.29%. In comparison to the RO model, the DRO model not only focuses on a single potential branch interruption scenario but also considers various non-worst-case scenarios as a basis for decision-making, leading to a total operation cost reduction of 12.85%.

5.2.2 Sensitivity Analysis of Ambiguity Set and Support Set

To further analyze the characteristics of the DRO model, we perform a sensitivity analysis by varying the confidence level γ of the ambiguity set and the control parameters Γ of the support set. The total cost in the out-of-sample test is evaluated for different values of γ and Γ. The results are summarized in Table 4.

Table 4
Costs under different confidence level γ and control parameters Γ (10^4\$)

γ \ Γ	Lower 20%	Lower 10%	Base	Upper 10%	Upper 20%
95%	11.849	12.268	13.766	14.678	15.572
90%	11.602	12.045	13.408	13.837	15.166
80%	11.048	11.773	13.256	13.562	14.768
70%	10.380	11.426	12.946	13.331	14.349

Under the same confidence level γ, as the support set control parameter Γ increases, the severity of secondary strikes in the worst-case distribution becomes more pronounced, leading to higher SR strategy formulation costs and unexpected load shedding penalty costs. The total cost increases by 13.11% or decreases by 13.92% when the base size of Γ increases or decreases by 20%, with the confidence level set at 95%. This indicates that the proposed DRO model develops better deployment strategies to cope with uncertainty. Higher Γ values make the model account for more severe scenarios, necessitating more robust and costlier strategies. Therefore, the proposed DRO model not only demonstrates economic benefits but also has a better ability to adapt to different fault scenarios, which explains its potential for application in actual scheduling under increasingly severe extreme events.

Under the same support set control parameter Γ, as the confidence level γ increases, the total cost of the DRO model continues to increase. This is due to the fact that, with higher confidence level γ, the Wasserstein metric model considers a broader range of potential distribution, even though the true distribution is not necessarily included. The worst-case distribution identified becomes more serious, leading to the highest total cost. This results in more conservative and robust SR strategies, which are costlier. With the total cost at the 95% confidence level increases by 6.33% compared to the cost at 70% confidence level, which demonstrates that scheduling decision-makers can adjust the confidence level γ to control the robustness of the SR strategy, highlighting the flexibility and controllability of the DRO model in actual scheduling scenarios.

5.3 Modified 33-bus and 32-node system

The case study in this section is conducted using the IEHS shown in Fig. 4, which comprises a modified IEEE 33-bus PDN and a Barry Island 32-node DHN, collectively referred to as the M33B32N system. In this setup, three CHP units are interconnected with buses 1, 22, and 33 in the PDN, and nodes 31, 1, and 32 in the DHN. Additionally, three EHs are connected to the same nodes as the CHP units. In this case study, the ambiguity set is constructed from 100 secondary strike samples. We observe that the maximum number of branch interruptions in the sample is 4, so N-4 unexpected branch outage events are considered here, and the parameter Γ in the support set is determined by the mean of the total outage duration in the sample, which is set to 60.

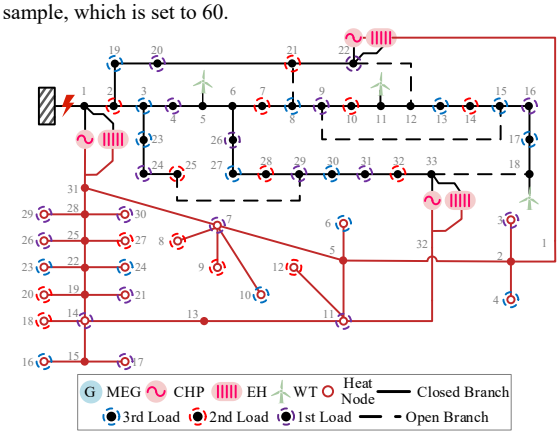

Fig. 4 The topology of M33B32N system

5.3.1 Effectiveness of VES in DHN

To illustrate the impact of the VES of the DHN in the SR strategy formulation of the IEHS, including the start/shut of CHP unit and EH unit and the reserve capacity, two case studies are set up for comparative analysis. The results generated by the two cases are verified in the 1000 MC simulating scenario.

Case V: Only the loss characteristics of the working fluid in the pipeline are considered, and the VES model is not included. The temperature change at the pipeline inlet is immediately reflected at the pipeline outlet, and the DHN does not exhibit the VES capacity.

Case VI: The VES model of the DHN and its capacity described in this paper are considered (i.e., the proposed).

The cost distribution of the two cases in the formulation and implementation process of the SR strategy is shown in Table 5. The thermal power balance of Case V and Case VI during the implement stage of the SR strategy is shown in Fig. 5.

In the Case V, shown in Fig. 5(a), due to the need to meet real-time source-load balance, although the thermal power provided by the CHP and EH units before the DRO model confirms the secondary strikes is less than that in Case VI, the thermal power supplied during the secondary strikes period is higher than in Case VI. The thermal power supplied by the CHP and EH units need to keep up with the thermal load trends. In each SR strategy implement period, the thermal power loss of DHN and the thermal load power need to be balanced, resulting in less flexibility in the SR strategy. A higher reserve capacity is required, and the CHP and EH units need to maintain long-term operation, which is reflected in the higher specific equipment operating costs shown in Table 5.

In Case VI, considering the thermal inertia of DHN and utilizing the VES capacity, during the period from 00:00 to 04:00, more CHP units and other heating equipment are invested in heating compared to Case V, shown in Fig. 5(b). This shows that the process of charging and discharging DHN as a large energy storage system in the SR strategy implement process, which can avoid the need for real-time source-load balance and extends this balance to a longer time scale. The flexible and adjustable characteristics of DHN are utilized to release its heating potential within the adjustable temperature range, ensuring that unexpected load shedding is minimized through long-term thermal power balance.

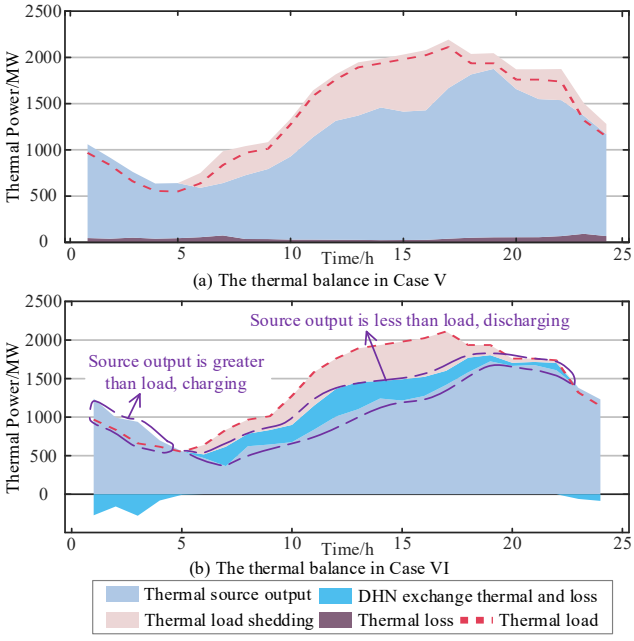

Fig. 5 The thermal power balance compared with Case V and Case VI

From the results in Table 5, considering the thermal inertia of DHN and utilizing the regulation capability of its VES, in the process of formulating the SR strategy, compared with Case V without considering, the deployment cost of CHP decreased by 4.86%, and the deployment cost of EH decreased by 7.66%. In the scenario considering VES capacity, the composite cross-time translation capability of VES ensures the synchronous change of electrical and thermal loads as much as possible, mitigating the issue of weak flexibility of CHP units.

5.3.2 Effectiveness of proposed SR strategy

To illustrate that the proposed SR strategy can overcome the limitations of a single SR strategy, three cases are set up in this section. The performance of these SR strategy based on the DRO model is tested using 1000 MC sampling to evaluate the effectiveness of the proposed SR strategy.

Case VII: In the SR formulation process, MEG is designated at a known bus, followed by the defensive MG reconfiguration deployment.

Case VIII: In the SR formulation process, both MEG allocation and reserve commitment are considered, but without defensive MG reconfiguration.

Case IX: The proposed strategy, which includes defensive MG reconfiguration in the PDN, along with MEG allocation and reserve commitment formulation.

Table 5
Equipment operating costs of Case V and Case VI under MC simulating scenario (10^4\$)

	CHP Start-Shut	CHP Reserve	EH Reserve	CHP Adjusting	EH Adjusting	Thermal Shedding	Total
Case V	2	7.98	2.87	13.31	4.78	9.83	40.77
Case VI	2	8.49	2.65	14.15	3.16	6.72	37.17

Fig. 6 compares the results of the PDS subsystem in the IEHS for MEG allocation and defensive MG reconfiguration between Case VII and Case IX in the SR strategy. The simulation results in the MC sampling scenarios are shown in Table 6.

Table 6
Costs of Case VII-IX under MC simulating scenario (10^4\$)

	Start-Shut	Reserve	Adjusting	Penalty	Total
Case VII	6	17.27	19.08	35.97	78.32
Case VIII	4.5	15.46	24.15	27.9	72.01
Case IX	4.5	14.68	22.32	27.89	69.39

In Case VII, the position of the MEG is specified before the SR decision is formulated, and the MG reconfiguration decisions are made with the MEG as the root bus. Although the radial topology of each MG is guaranteed, the load distribution within each MG is not balanced, preventing the CHP unit from being fully utilized to maximize support for critical loads. The uneven output of the CHP unit leads to a decrease in thermal power output, causing branch outages in the PDN to propagate to the DHN through deep IEHS coupling. Consequently, the formulation of the SR strategy requires a higher cost of start-up and greater reserve capacity in Case VII, but it does not effectively reduce the unexpected load shedding penalty costs during the SR implementation process.

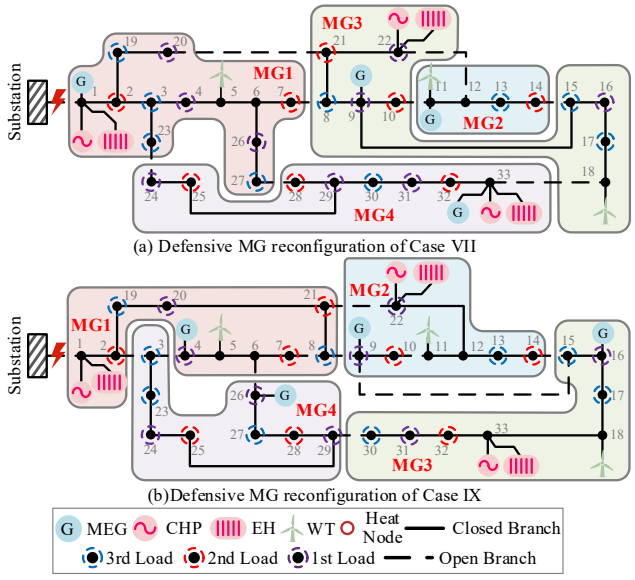

Fig. 6 The comparison of defensive MG reconfiguration

In the SR strategy of Case IX, the allocation strategy of MEG is carried out simultaneously with defensive MG reconfiguration and reserve commitment. The MEG can identify buses with the highest priority and the heaviest load rates. Especially when combined with defensive MG reconfiguration, it ensures that the total load in each MG matches the supply capacity by adjusting the location of the MEG access bus and MG boundaries, maximizing the utilization of MEG capacity. The rational use of MEG allocation through the SR strategy, which incorporates the co-optimization of defensive MG reconfiguration, MEG allocation, and reserve commitment, results in a more economical SR strategy formulation cost, reducing the unexpected load shedding by 1705MW compared to Case VII. This demonstrates the superiority of the proposed SR strategy, as it effectively allocates the limited emergency resources of the IEHS to the greatest extent.

Fig. 7 illustrates the reserve commitment of the SR strategy for Case VIII and Case IX, along with the total generation power of the MEG in the MC simulation scenario. The worst-case probability distribution of future uncertain secondary strikes captured by the DRO model shows that the first branch outage occurs at 4:00. In Case IX, prior to this initial branch outage, no reserve capacity preparation is conducted, and the MEG maintains a stable output. During this period, the CHP unit generates substantial thermal power to maximize the temperature of the DHN, adjusting for load fluctuations.

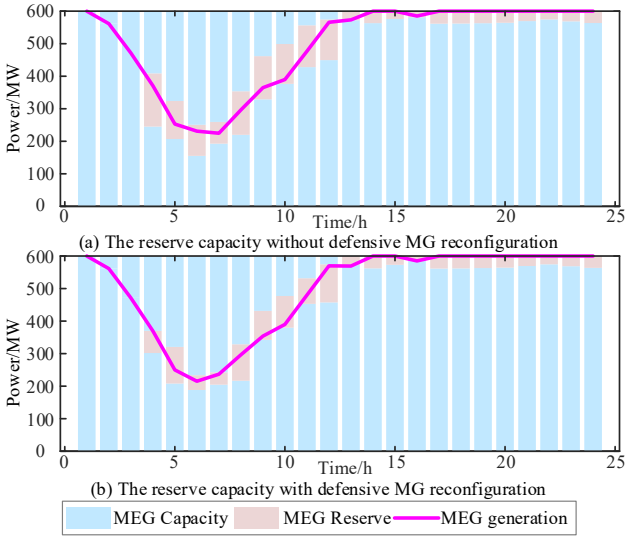

Fig. 7 The comparison reserve commitment between Case VIII and IX

After 4:00, when the first branch outage impact occurs, the MEG unit establishes a corresponding reserve capacity. As secondary strikes continue and load power increases, the MEG's reserve capacity gradually expands until it reaches the power output boundary, beyond which it cannot be increased further. In the MC simulation scenario, after multiple serious branch outages, the MEG sustains its maximum output within the reserve capacity during load peaks, thereby maximizing support for critical loads.

Both Case VIII and Case IX include reserve commitments, but Case VIII does not involve defensive MG reconfiguration. While Case VIII utilizes the DRO model to obtain the worst distribution of subsequent branch outage scenarios, it relies on increasing the reserve capacity to manage these outages effectively. This approach is constrained by the ramping capabilities of the MEG unit and the need to balance the formulation cost of the SR strategy with the unexpected load shedding penalty cost.

Consequently, Case VIII requires a higher reserve capacity compared to Case IX.

This increased reserve capacity in Case VIII arises from the absence of defensive MG reconfiguration. Maintaining the entire PDN in an integrated topology allows the MEG to maximize its supply capacity before secondary strikes occur, facilitating energy mutual aid within the network. However, in practical applications, the capacity of the MEG is significantly smaller than the total network load, as set up in this case study. Thus, integrating multiple MGs into a single topology provides only limited benefits.

When secondary strikes occur, the sudden disconnection of lines results in all loads at the endpoints being detached. To maintain source-load balance and ensure voltage stability at both ends of the disconnected line, the MEG must quickly adjust its output. This necessitates substantial reserve capacity and rapid output fluctuations to coordinate with remaining units during such emergencies, which conflicts with the MEG units' goal of maximizing output in extreme branch outage scenarios to protect critical loads effectively.

6. Conclusion

This study proposes a novel DRO-based SR strategy for IEHS and constructs appropriate ambiguity set and support set to capture the uncertainty of branch outages caused by secondary strikes during SR implementation. The logical constraint convex relaxation, along with an improved C&CG algorithm, is integrated into the DRO model formulation to address the challenge of solving the SR problem. The effectiveness of the proposed SR strategy and DRO model for IEHS is verified using two test systems. Compared to existing SR strategies, the coordinated SR strategy for IEHS reduces the unexpected load shedding by up to 1705MW during secondary strikes. Additionally, the DRO model demonstrates lower operation costs under secondary strikes, outperforming other models by more than 10.29%. We selected 20 different parameter configurations for the proposed DRO model's sensitivity analysis. Compared to the rate of parameter changes, the rate of operating cost variation is lower, demonstrating that the DRO-based SR strategy for IEHS maintains stable performance across different confidence levels and control parameters, underscoring its potential for practical industrial applications.

Further research is recommended in the following areas: 1) While this paper focuses on the uncertainty of subsequent unexpected events, uncertainties in renewable energy generation and load consumption during SR implementation process are also significant. Future work will consider incorporating these uncertainties into the model. 2) This paper assumes a three-phase balanced state for the PDS, yet addressing the three-phase imbalance problem during SR implementation is crucial in practice. 3) This current focuses on the operational scheduling in SR, but integrating emergency crew dispatch and fault components repair will be an essential direction for future research.

Acknowledgements

This work is supported by National Natural Science Foundation of China (U22B2098)

Appendix. DRO reformulation

This section provides the derivation process from Eq.(60) to Eq.(61).

Step 1. Reformulate Eq.(60) to a worst-case constrained optimization problem:

$$\begin{aligned} &\min_{\beta\geq 0,\alpha_s} \quad \sum_{s=1}^{Ns} p_s\alpha_s + \beta\theta \\ &s.t. \quad \alpha_s \geq \max_{\boldsymbol{\xi}\in\Xi}\left[\mathcal{Q}(\boldsymbol{x},\boldsymbol{i},\boldsymbol{\xi}) - \beta\left\|\boldsymbol{\xi}-\hat{\boldsymbol{\xi}}^s\right\|\right], \quad \forall\boldsymbol{\xi}\in\Xi, \forall s=1,\ldots,Ns \end{aligned} \tag{63}$$

Step 2. According to transformation mentioned in Ref.[41], the norm operation in the right-hand side of Eq.(63) can be reformulated into a linear operation by introducing auxiliary variables κ_s:

$$\max_{\boldsymbol{\xi}\in\Xi}\left[\mathcal{Q}(\boldsymbol{x},\boldsymbol{i},\boldsymbol{\xi}) - \max_{\|\kappa_s\|_*^p\leq\beta} \kappa_s^{\mathrm{T}}\left(\boldsymbol{\xi}-\hat{\boldsymbol{\xi}}^s\right)\right] \tag{64}$$

According to the definition of dual norm:

$$\left\|\boldsymbol{\xi}-\hat{\boldsymbol{\xi}}^s\right\| = \max_{\|\kappa_s\|_*^p\leq 1} \kappa_s^{\mathrm{T}}\left(\boldsymbol{\xi}-\hat{\boldsymbol{\xi}}^s\right) \tag{65}$$

Where, $\|\cdot\|_*$ represents the dual norm operation. For L_1-norm, its dual norm is the L_∞-norm. Conversely, for the L_∞-norm, its dual norm is the L_1-norm. Additionally, the dual norm of the L_2-norm is itself.

Step 3. Converting the maximization operation to the minimization operation and removing the minus sign can keep the optimization direction unchanged.

$$\max_{\boldsymbol{\xi}\in\Xi}\min_{\|\kappa_s\|_*^p\leq\beta}\left[\mathcal{Q}(\boldsymbol{x},\boldsymbol{i},\boldsymbol{\xi}) - \kappa_s^{\mathrm{T}}\left(\boldsymbol{\xi}-\hat{\boldsymbol{\xi}}^s\right)\right] \tag{66}$$

Step 4. Based on the minimax theorem, the Eq.(66) can be written as:

$$\min_{\|\kappa_s\|_*^p\leq\beta}\max_{\boldsymbol{\xi}\in\Xi}\left[\mathcal{Q}(\boldsymbol{x},\boldsymbol{i},\boldsymbol{\xi}) - \kappa_s^{\mathrm{T}}\left(\boldsymbol{\xi}-\hat{\boldsymbol{\xi}}^s\right)\right] \tag{67}$$

REFERENCES

[1] Executive Office of the President, Washington, DC, USA, Economic benefits of increasing electric grid resilience to weather outages, 2013. [Online]. Available: https://www.energy.gov/downloads/economic-benefitsincreasing-electric-grid-resilience-weather-outages

[2] Salim N A, Jasronita J, and Muhammad M O. Reliability assessment by sensitivity analysis due to electrical power sequential tripping for energy sustainability. International Journal of Electrical Power & Energy Systems 2021; 126: 106582.

[3] Wang K, Xue Y, Guo Q, et al. A Coordinated Reconfiguration Strategy for Multi-Stage Resilience Enhancement in Integrated Power Distribution and Heating Networks. IEEE Transactions on Smart Grid 2022; 14(4): 2709-2722.

[4] The February 2021 cold weather outages in texas and the south central United States. Accessed: Feb. 2021. [Online]. Available: https://www.ferc.gov/media/february-2021-cold-weather-outages-texas-and-southcentral-united-states-ferc-nerc-and

[5] Lei S, Chen C, Song Y, Hou Y. Radiality Constraints for Resilient Reconfiguration of Distribution Systems: Formulation and Application to Microgrid Formation. IEEE Transactions on Smart Grid 2020; 11: 3944–56.

[6] Bian Y, Chen C, Huang Y, Bie Z, Catalão JPS. Service Restoration for Resilient Distribution Systems Coordinated With Damage Assessment. IEEE Transactions on Power Systems 2022; 37: 3792–804.

[7] Cai S, Zhang M, Xie Y, Wu Q, Jin X, Xiang Z. Hybrid Stochastic-Robust Service Restoration for Wind Power Penetrated Distribution Systems Considering Subsequent Random Contingencies. IEEE Trans Smart Grid 2022; 13: 2859–72.

[8] Hussain A, Bui V H, Kim H M, A Resilient and Privacy-Preserving Energy Management Strategy for Networked Microgrids. IEEE Transactions on Smart Grid 2016; 9(3): 2127-2139.

[9] Shen F, López J C, Wu Q, et al, Distributed Self-Healing Scheme for Unbalanced Electrical Distribution Systems Based on Alternating Direction Method of Multipliers, IEEE Transactions on Power Systems 2020; 35(3): 2190-2199.

[10] Kim Y J, Wang J, Lu X, A Framework for Load Service Restoration Using Dynamic Change in Boundaries of Advanced Microgrids With Synchronous-Machine DGs, IEEE Transactions on Smart Grid 2018; 9(4): 3676-3690.

[11] Lei S, Wang J, Hou Y. Remote-Controlled Switch Allocation Enabling Prompt Restoration of Distribution Systems. IEEE Transactions on Power Systems 2018; 33: 3129-3142.

[12] Liu J, Qin C, Yu Y. Enhancing Distribution System Resilience With Proactive Islanding and RCS-Based Fast Fault Isolation and Service Restoration. IEEE Transactions on Smart Grid 2020; 11: 2381-2395.

[13] Wu W, Hou H, Zhu S, et al. An intelligent power grid emergency allocation technology considering secondary disaster and public opinion under typhoon disaster. Applied Energy 2024; 353: 122038.

[14] Che L, Shahidehpour M. Adaptive formation of microgrids with mobile emergency resources for critical service restoration in extreme conditions. IEEE Transactions on Power Systems 2018; 34(1): 742-753.

[15] Yao, S, Wang P, Liu X, et al. Rolling optimization of mobile energy storage fleets for resilient service restoration. IEEE Transactions on Smart Grid 2019; 11(2): 1030-1043.

[16] Erenoğlu, Ayşe Kübra, Terzi İ S, et al. Resiliency-driven multi-step critical load restoration strategy integrating on-call electric vehicle fleet management services. IEEE Transactions on Smart Grid 2022; 13(4): 3118-3132.

[17] Ghasemi S, Moshtagh J. Distribution system restoration after extreme events considering distributed generators and static energy storage systems with mobile energy storage systems dispatch in transportation systems. Applied Energy 2022; 310: 118507.

[18] Lei S, Chen C, Li Y, et al. Resilient Disaster Recovery Logistics of Distribution Systems: Co-Optimize Service Restoration With Repair Crew and Mobile Power Source Dispatch. IEEE Transactions on Smart Grid 2019; 10: 6187-202.

[19] Hou H, Tang J, Zhang Z, et al. Stochastic pre-disaster planning and post−disaster restoration to enhance distribution system resilience during typhoons. Energy Conversion and Economics 2023; 4(5): 346-363.

[20] Wikipedia, Hurricane Sandy, Sep. 2024. [Available] https://en.wikipedia.org/wiki/Hurricane_Sandy

[21] North American Electric Reliability Corporation, Hurricane Harvey Event Analysis Report, March, 2018. [Available] https: //www. nerc. com/pa/rrm/ea/Hurricane_Harvey_EAR_DL/NERC_Hurricane_Harvey_EAR_20180309.pdf

[22] S. Cai, Y. Xie, Q. Wu, et al. Distributionally Robust Microgrid Formation Approach for Service Restoration Under Random Contingency, IEEE Transactions on Smart Grid 2021, 12(6): 4926-4937

[23] Typhoon Faxai Pummels Tokyo Area, Sep. 2019. [Available] https://www.nesdis.noaa.gov/news/typhoon-faxai-pummels-tokyo-area.

[24] Ma L, Hui H, Wang S, et al. Coordinated optimization of power-communication coupling networks for dispatching large-scale flexible loads to provide operating reserve. Applied Energy 2024; 359: 122705.

[25] Zhao T, Zhang H, Liu X, et al. Resilient unit commitment for day-ahead market considering probabilistic impacts of hurricanes. IEEE Transactions on Power Systems 2020; 36(2): 1082-1094.

[26] Nitsch F, Deissenroth-Uhrig M, Schimeczek C, et al. Economic evaluation of battery storage systems bidding on day-ahead and automatic frequency restoration reserves markets. Applied Energy 2021; 298: 117267.

[27] Cremoncini D, Frate G F, Bischi A, et al. Optimal participation of a wind and hybrid battery storage system in the day-ahead and automatic frequency restoration reserve markets. Journal of Energy Storage 2024; 94: 112309.

[28] Wang K, Xue Y, Zhou Y, et al. Distributed coordinated reconfiguration with soft open points for resilience-oriented restoration in integrated electric and heating systems. Applied Energy 2024; 365: 123207.

[29] Yin X, Ye C, Ding Y, et al. Combined Heat and Power Dispatch Against Cold Waves Utilizing Responsive Internet Data Centers. IEEE Transactions on Sustainable Energy 2023; 1–15.

[30] Tao R, Zhao D, Xu C, et al. Resilience Enhancement of Integrated Electricity-Gas-Heat Urban Energy System With Data Centres Considering Waste Heat Reuse. IEEE Transactions on Smart Grid 2023; 14: 183–98.

[31] Li Z, Wu W, Shahidehpour M, et al. Combined Heat and Power Dispatch Considering Pipeline Energy Storage of District Heating Network. IEEE Transactions on Sustainable Energy 2016; 7: 12-22.

[32] Huang W, Zhang X, Li K, et al. Resilience Oriented Planning of Urban Multi-Energy Systems With Generalized Energy Storage Sources. IEEE Transactions on Power Systems 2022; 37: 2906-2918.

[33] Bu Y, Yu H, Ji H, et al. Hybrid data-driven operation method for demand response of community integrated energy systems utilizing virtual and physical energy storage. Applied Energy 2024; 366: 123295.

[34] Ding T, Qu M, Wang Z, et al. Power System Resilience Enhancement in Typhoons Using a Three-Stage Day-Ahead Unit Commitment. IEEE Transactions on Smart Grid 2021; 12(3): 2153-2164.

[35] Cai S, Xie Y, Wu Q, et al. Active and Reactive Power Coordinated Two-Stage MG Scheduling for Resilient Distribution Systems Under Uncertainties. IEEE Transactions on Smart Grid 2022; 13: 2986–98.

[36] Zhu, Rujie, Hua Wei, Xiaoqing Bai. Wasserstein metric based distributionally robust approximate framework for unit commitment. IEEE Transactions on Power Systems 2019; 34(4): 2991-3001.

[37] He C, Zhang X, Liu T, et al. Distributionally Robust Scheduling of Integrated Gas-Electricity Systems With Demand Response. IEEE Transactions on Power Systems 2019; 34(5): 3791-3803.

[38] Zheng X, Qu K, Lv J, et al. Addressing the Conditional and Correlated Wind Power Forecast Errors in Unit Commitment by Distributionally Robust Optimization. IEEE Transactions on Sustainable Energy 2021; 12(2): 944-954.

[39] Li X, Han B, Li G, et al. Dynamic Topology Awareness in Active Distribution Networks Under DG Uncertainties Using GMM-PSEs and KL Divergence. IEEE Transactions on Sustainable Energy 2021; 12(4): 2086-2096.

[40] Cao Y, Wei W, Chen L, et al. Supply Inadequacy Risk Evaluation of Stand-Alone Renewable Powered Heat-Electricity Energy Systems: A Data-Driven Robust Approach. IEEE Transactions on Industrial Informatics 2021; 17(3): 1937-1947.

[41] Zhou Y, Wei Z, Shahidehpour M, et al. Distributionally Robust Resilient Operation of Integrated Energy Systems Using Moment and Wasserstein Metric for Contingencies. IEEE Transactions on Power Systems 2021;

36: 3574-3584.

[42] Zhou Y, Li X, Han H, et al. Resilience-oriented planning of integrated electricity and heat systems: A stochastic distributionally robust optimization approach. Applied Energy 2024; 353: 122053.

[43] Duan C, Fang W, Jiang L, et al. Distributionally robust chance-constrained approximate AC-OPF with Wasserstein metric. IEEE Transactions on Power Systems 2018; 33(5): 4924-4936.

[44] Pang, Kaiyuan, et al. Formulation of radiality constraints for optimal microgrid formation. IEEE Transactions on Power Systems 2022; 38(6): 5341-5355.

[45] Xiong H, Yan M, Guo C, et al. DP based multi-stage ARO for coordinated scheduling of CSP and wind energy with tractable storage scheme: Tight formulation and solution technique. Applied Energy 2023, 333: 120578.

[46] G McCormick. Computability of Global Solutions to Factorable Nonconvex Programs: Part I Convex Underestimating Problems. Mathematical Programming 1976; 10: 147-175.